Energy Conversion and Management: X 31 (2026) 101957

Contents lists available at ScienceDirect

Energy Conversion and Management: X

journal homepage: www.sciencedirect.com/journal/energy-conversion-and-management-x

# Impact of renewable energy resource endowment on capacity configuration optimization for wind-solar-storage-transmission systems

You Zhou [a,b], Hao He [a], Shaohui Zhang [c], Fuwenxin Yu [a], Bowen Yi [a,d,*]

[a] School of Economics & Management, Beihang University, Beijing, China
[b] CCTEG Ecological Environment Technology Co., Ltd., Beijing, China
[c] International Institute for Applied Systems Analysis, Laxenburg, Austria
[d] MOE Laboratory for Low-carbon Intelligent Governance (LLIG), Beihang University, Beijing, China

ARTICLE INFO

*Keywords:*
Renewable energy
Energy storage
Electricity transmission
Capacity configuration

ABSTRACT

As thermal power is gradually phased out, renewable energy bases dominated by wind and solar power will require energy storage to replace the current practice of bundling renewables with thermal power for long-distance transmission. This transition raises a new challenge: determining the most cost-effective capacity configuration for Wind-Solar-Storage-Transmission (WSST) systems, which depends critically on regional wind and solar resource conditions. This study investigates the fundamental relationship between resource conditions and the optimal capacity configuration of renewable energy bases. To this end, 210 sites across five major power-exporting provinces in North China are selected as research subjects. Drawing on hourly wind and solar capacity factor data covering 87,600 h from 2014 to 2023, we develop both a basic optimization model and a scenario-based distributionally robust optimization model for WSST systems. These models are used to examine how renewable energy intermittency, regional heterogeneity, and resource uncertainty shape the cost-optimal capacity allocation of renewable energy bases. The results show that the installed capacities of wind and solar power are strongly correlated with their respective resource endowments and, beyond competing with each other, also exhibit pronounced complementarity. At current storage prices, not all renewable bases require energy storage; the key determinant is the wind-to-solar capacity factor ratio. Compared with wind, solar PV depends far more heavily on storage. In single-source scenarios, higher solar capacity factors correspond to greater storage requirements, with better solar resources further amplifying this demand, whereas wind power requires little to no storage regardless of resource conditions. In wind-solar complementary systems, storage capacity follows an inverted U-shaped pattern with respect to the wind-to-solar capacity factor ratio. Transmission capacity is primarily driven by wind resources, while solar conditions exert a comparatively minor influence. Given the higher uncertainty associated with wind power, explicitly accounting for resource variability generally leads to reduced wind capacity, increased solar PV capacity, unchanged storage, and lower transmission capacity.

## 1. Introduction

Variable renewable energy sources, primarily wind and solar power, have been widely deployed worldwide and are emerging as potentially dominant components of future energy systems. However, their inherent characteristics also pose new challenges to power systems, the two most significant being intermittency and spatial heterogeneity [1]. A globally common phenomenon is the inverse distribution pattern between renewable energy resources and load centers [2]. In pursuit of higher capacity factors, some countries have established large-scale renewable energy bases in remote areas and transmit the generated electricity to load centers via high-voltage transmission lines [3]. The most typical example is China, which, owing to its vast territory and advanced ultra-high-voltage (UHV) transmission technology, often delivers electricity from the renewable-rich northwest to the central and eastern regions over thousands of kilometers of transmission lines [4].

Current renewable energy bases are typically paired with thermal power plants and delivered as a bundled power supply. This approach is mainly intended to maximize the utilization of transmission corridors and to provide a more stable supply that is more acceptable to receiving regions. Under the carbon neutrality strategy, however, thermal power is bound to gradually exit the power system, rendering the existing

* Corresponding author at: School of Economics & Management, Beihang University, Beijing, China.
*E-mail address:* ybw2018@buaa.edu.cn (B. Yi).

https://doi.org/10.1016/j.ecmx.2026.101957
Received 12 April 2026; Received in revised form 11 May 2026; Accepted 12 May 2026
Available online 15 May 2026

bundling mode for renewable energy bases unsustainable [5]. To facilitate the economic integration of renewables, these bases are increasingly expected to be equipped with energy storage, especially electrochemical storage, which is not constrained by geographical conditions [6].

Yet because resource characteristics differ across regions, some renewable energy bases rely solely on wind or solar power, while others integrate both. Even in the latter case, there are variations in which resource is more abundant, along with differences in volatility, seasonality, and other micro-level attributes [7]. It therefore remains uncertain whether all renewable energy bases need to be equipped with storage, and what the optimal storage capacity should be. Whether the integration of storage would in turn affect the optimal transmission capacity of power export corridors also requires further clarification. These uncertainties give rise to the problem of optimal capacity configuration in Wind-Solar-Storage-Transmission (WSST) systems, which aims to economically integrate renewable energy from resource-rich regions [8]. The most critical factor shaping this problem is the inherent characteristics of renewable energy resources themselves.

The optimal configuration of renewable energy and storage has been widely discussed in the literature [9,10]. Wang et al. [11] developed a refined rolling optimization strategy for the coordinated operation of a renewable-powered green hydrogen production system with multiple electrolyzers and battery storage. Ghanbari et al. [12] optimized the design, sizing, and technology selection of a hybrid renewable microgrid comprising batteries, wind turbines, and photovoltaic panels. Ruggles et al. [13] examined how the length of historical weather data used in designing least-cost wind, solar, and storage systems affects resource adequacy, finding that highly reliable systems require longer data records, while fewer years may suffice when traditional dispatchable generation is incorporated. Other studies have investigated the role of power transmission in integrating renewables [14–16], and several have further examined the electricity delivery problem of renewable energy bases equipped with storage. For instance, Göke et al. [17] used a comprehensive capacity expansion model based on the AnyMOD framework to compare planning approaches for a fully renewable energy system in Germany, incorporating detailed spatial and temporal factors, energy exchanges with the rest of Europe, and demand from various sectors. Artis et al. [18] presented a multi-objective model for contingency-constrained transmission expansion planning that incorporates large-scale hydrogen and compressed-air storage as well as wind and solar farms to enhance supply–demand balance and grid flexibility. Ma and Liu [19] developed an optimal capacity configuration and short-term coordination strategy for hydro-wind-PV systems that accounts for UHV transmission and reservoir operation, applying it to a case study in Qinghai, China. Sun et al. [20] proposed a two-layer capacity planning model for large-scale wind-photovoltaic-pumped hydro storage bases integrated with UHV direct current transmission lines, also focusing on Qinghai.

While these studies offer valuable perspectives, two important gaps remain. First, existing work is largely confined to case studies of individual regions or projects, and offers limited insight into the general patterns through which resource characteristics and regional heterogeneity shape the capacity configuration of WSST systems. As a result, the literature provides little guidance on how findings from one region can be transferred to renewable bases located in fundamentally different resource environments. Second, the characterization of renewable energy uncertainty in this strand of literature remains relatively weak, with limited in-depth discussion of how long-term resource variability affects the robustness of optimal capacity configurations. Most robustness analyses in this area have focused on short-term, micro-scale power dispatch rather than long-term capacity planning [21–25].

To address these gaps, this study selects 210 sites across five major power-exporting provinces in North China as research objects, and draws on wind and solar capacity factor data covering 87,600 h from 2014 to 2023. Building on this dataset, we develop a basic optimization model and a distributionally robust optimization model for WSST systems to investigate how renewable energy intermittency, regional heterogeneity, and resource uncertainty jointly shape the optimal capacity configuration of renewable energy bases. The main contributions of this study, which distinguish it from existing work, are threefold. First, in contrast to the case-specific focus of prior studies, we leverage extensive point-source resource data from 210 sites to systematically identify the general patterns through which renewable resource endowments influence the capacity configuration of WSST systems, generating cross-regional insights that are transferable to other resource-rich exporting regions. Second, in contrast to existing robustness studies that concentrate on short-term dispatch, we construct a scenario-based distributionally robust optimization model driven by ten years of long-term resource data, and use it to characterize the optimal WSST capacity configuration under renewable energy uncertainty at the planning timescale. Third, by jointly examining wind, solar, storage, and transmission within a unified framework, we uncover several counterintuitive mechanisms, including the inverted U-shaped relationship between storage capacity and the wind-to-solar capacity factor ratio, and the asymmetric storage dependence of wind versus solar power. These findings provide scientific support for planning the most cost-effective construction configurations of renewable energy export bases in regions with differing resource endowments.

The remainder of this study is organized as follows. Section 2 describes the optimization methods developed for the WSST system. Section 3 presents the data sources in detail. Sections 4 and 5 discuss the results of the basic optimization model and the distributionally robust optimization model, respectively. Section 6 concludes.

## 2. Methods

This study constructs a Wind-Solar-Storage-Transmission (WSST) system to simulate the optimal capacity decisions of a power export base. The model considers two regions: an export region and an import region. The export region generates electricity from wind, solar photovoltaic (PV), and energy storage facilities, and delivers it through transmission lines to meet the electricity demand of the import region. The export region therefore operates as a zero-carbon power system. When a supply–demand mismatch occurs, the import region may also procure local electricity to fulfill its needs; rather than modeling the specific sources of this local supply, we represent its cost through a time-varying electricity price.

The model makes decisions on the installed capacities of power generation, energy storage, and transmission lines at the macroscopic timescale, while simultaneously optimizing real-time dispatch, charging and discharging strategies, and local electricity purchases at the microscopic timescale. The objective is to identify the cost-minimal configuration for the export region while ensuring that the electricity demand of the import region is fully met.

The methodological framework is illustrated in Fig. 1 and comprises a deterministic basic optimization model and a scenario-based distributionally robust optimization model. Because the basic model is computationally lighter, we apply it to large-scale simulations across numerous sites to investigate how renewable resource endowments shape the optimal capacity configuration of the WSST system. Building on a subset of representative sites, we then employ the distributionally robust optimization model to examine how long-term uncertainty in renewable energy generation affects the optimal capacity configuration.

### 2.1. Basic optimization model

#### 2.1.1. Renewable generation constraints

The system primarily depends on solar plants and wind farms for power generation, serving as the main sources to meet electricity demand at the receiving end. Equations (1) and (2) define the output limits for these variable renewable energy sources.

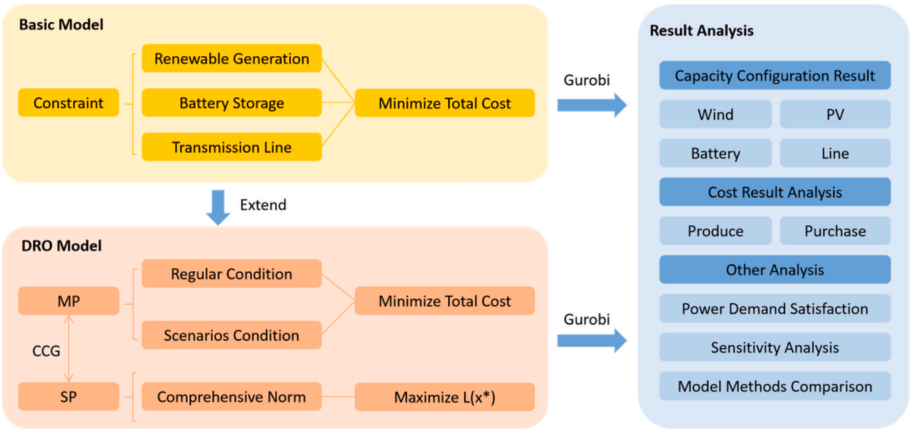


**Fig. 1.** Conceptual framework of this method.

$$p_t^{we} + p_t^{wg} \le K_t^W \cdot P^W \tag{1}$$

$$p_t^{se} + p_t^{sg} \le K_t^S \cdot P^S \tag{2}$$

$$p_t^{we}, p_t^{wg}, p_t^{se}, p_t^{sg} \ge 0 \tag{3}$$

where $K_t^W$ and $K_t^S$ represent the capacity factor of wind or solar PV. Decision variables include power from wind farms to storage units ($p_t^{we}$) or the grid ($p_t^{wg}$), power from solar plants to storage units ($p_t^{se}$) or the grid ($p_t^{sg}$), and the capacity of wind farms ($P^W$) and solar plants ($P^S$).

#### 2.1.2. Battery storage constraints

Battery energy storage systems can rapidly store and release energy in response to fluctuations in grid load, helping to balance the gap between power supply and demand. Equations (4) and (5) characterize the dynamic process and allowable range of the state of charge, while Equation (6) identifies the sources of charging. Equations (7) and (8) define the feasible limits for charging and discharging operations.

$$W_{t+1} = W_t + \left(p_t^c \cdot \eta_c - p_t^{dc} / \eta_{dc}\right) \cdot \tau \tag{4}$$

$$0 \le W_t \le P^E \tag{5}$$

$$p_t^{we} + p_t^{se} = p_t^c \tag{6}$$

$$0 \le p_t^c \le \gamma \cdot P^E \tag{7}$$

$$0 \le p_t^{dc} \le \gamma \cdot P^E \tag{8}$$

where $\eta_c$ and $\eta_{dc}$ represent the charging or discharging efficiency. $\tau$ denotes the duration of period $t$. $\gamma$ indicates the maximum power-capacity coefficient of battery. $P^E$ is the energy capacity of the storage unit, which varies with the battery size. Decision variables include charging ($p_t^c$) or discharging power ($p_t^{dc}$), as well as the state-of-charge ($W_t$).

Due to energy losses during charging and discharging, simultaneously scheduling these operations is not cost-effective. Therefore, the optimal scheduling strategy adheres to this constraint $p_t^c \cdot p_t^{dc} = 0$.

#### 2.1.3. Transmission line constraints

Ultra-high voltage transmission lines facilitate long-distance electricity transmission with high efficiency, minimizing energy losses and playing a vital role in large-scale inter-regional power delivery. Equations (9) and (10) define the composition and capacity limits of transmitted energy, while Equation (11) specifies how this energy is utilized to meet the power demand at the receiving end.

$$p_t^{wg} + p_t^{sg} + p_t^{dc} = p_t^g \tag{9}$$

$$0 \le p_t^g \le P^L \tag{10}$$

$$p_t^g + p_t^{pur} = p_t^{local} \tag{11}$$

$$p_t^{pur} \ge 0 \tag{12}$$

where $P^L$ denotes the capacity of power transmission line. $p_t^g$ denotes the total power transmitted to the grid. $p_t^{pur}$ indicates the purchased power on the demand side, and $p_t^{local}$ represents the total power demand.

#### 2.1.4. Objective function

The objective function of the model is to minimize the total cost ($C^{TOT}$) of ensuring power supply over the study period, including the construction costs of wind power, solar PV, energy storage, and transmission lines, as well as the direct electricity purchase cost on the demand side, as shown in Equation (13).

$$\begin{cases} \min C^{TOT} = P^E \cdot C^E + P^L \cdot C^L + P^W \cdot C^W + P^S \cdot C^S + \sum_{t=1}^{T} \left(P_t^{pur} \cdot C_t^{pur}\right) \\ s.t. Equations(1) - (12) \end{cases} \tag{13}$$

where $C^W$, $C^S$, $C^E$, $C^L$ respectively represent the annualized unit construction costs of wind power, solar PV, energy storage, and power transmission lines. $C_t^{pur}$ denotes the direct electricity purchase cost, which varies over time.

### 2.2. Distributionally robust optimization model

This study employs a scenario-based distributionally robust optimization (DRO) model to account for the long-term variability of renewable energy resources. The DRO framework allows us to derive a capacity configuration that remains resilient across a wide range of plausible future resource conditions [26], which is essential because traditional optimization methods typically rely on deterministic assumptions or overly simplified stochastic representations and may fail to capture long-cycle resource variability [27]. By applying DRO, the optimized configuration is not only cost-effective but also well adapted to the intermittent and uncertain nature of renewable resources over extended time horizons.

Specifically, the ambiguity set in our model is constructed over the probability weights assigned to a finite collection of annual scenarios, where each scenario corresponds to one calendar year of historical hourly capacity factors. The model therefore performs a robust reweighting of historical resource years, placing our formulation within

the well-established class of scenario-based DRO. We adopt this formulation, rather than alternatives such as a Wasserstein ball or a moment-based ambiguity set, because the relevant uncertainty for long-term capacity planning is inter-annual variability in resource conditions rather than short-term stochasticity. Each annual scenario retains the full 8,760-hour time series, so the marginal distribution, intra-day fluctuations, seasonality, wind-solar correlation, and extreme periods are preserved as raw historical trajectories. With ten years of hourly data, the marginal distribution of capacity factors is already densely sampled; what is genuinely scarce is the number of distinct resource years, which is precisely the dimension along which annual-scenario reweighting places its ambiguity. Reweighting full historical years also preserves the temporal coherence on which storage sizing and reliability evaluation depend, whereas ambiguity constructed in the capacity factor space would generally break the wind-solar and hour-to-hour coupling.

#### 2.2.1. Model frame of DRO

In Section 2.1, the variables are categorized into two types: first-stage and second-stage variables. First-stage variables, denoted by $x$ , remain unchanged across different scenarios and primarily represent the capacities of various technologies in this study. Second-stage variables, denoted by $y$, are adjustable based on specific scenarios, such as electricity purchase on the demand side. The deterministic model introduced in Section 2.1 can be formulated in matrix form, as shown in Equations (14)-(19).

$$\min a^T x + b^T y \tag{14}$$

$$Ax \le c \tag{15}$$

$$Bx + Cy \le d \tag{16}$$

$$\xi x + Dy \le e \tag{17}$$

$$Ey \le f \tag{18}$$

$$Fy = g \tag{19}$$

Equation (14) is the expression of the objective function, which includes both first-stage and second-stage variables, corresponding to Equation (13). $a^T x$ is the construction cost, and $b^T y$ is the cost of purchasing electricity on the demand side. Equations (15) and (16) represent the constraint relationships of the first-stage variables, corresponding to Equations (5), (7), (8), and (10). In the DRO model, the capacity factors of wind power and PV are transformed from parameters into uncertain variables, denoted by matrix $\xi$. Equation (17) includes the constraint relationships between the first-stage variables and the uncertain variables, corresponding to Equations (1) and (2). Equations (18) and (19) are constraint relationships involving only the second-stage variables, corresponding to Equations (3), (4), (6), (9), (11), and (12).

From Equations (14) to (19), it can be seen that the uncertain variables exist only in the constraint conditions, which include both first-stage and second-stage variables. Therefore, we construct a two-stage distributionally robust capacity planning model. In the first stage, the optimization focuses on the total construction cost, where $x$ represents the first-stage variables. In the second stage, the model needs to optimize the expected cost under uncertain variables $\xi$, which can yield the worst-case power output given the values of the first-stage decision variables. The model can be expressed as follows:

$$\min_{x \in X} a^T x + \max_{P(\xi) \in \Omega} E_P\left(b^T y\right) \tag{20}$$

where $X$ represents the feasible region constructed by Equation (15). $P(\xi)$ denotes the probability distribution function of the uncertain parameter. $E_P(\cdot)$ denotes the calculation of the expected value of the probability distribution function. $\Omega$ represents the distribution set of the uncertain.

In practice, obtaining the uncertainty distribution set $\Omega$ is challenging, and a feasible solution is to select discrete scenarios. By using $K$ actual scenarios derived from historical data, the number of discrete scenarios is limited. Consequently, the model is further formulated as follows:

$$\min_{x \in X} a^T x + \max_{\{p_k\} \in \Omega} \sum_{k=1}^{K} \left( p_k \cdot \min_{y_k \in Y(x, \xi_k)} \left(b^T y_k\right) \right) \tag{21}$$

Here, $\{p_k\}$ represents the probability distribution value of the discrete scenario. The purpose of the max is to find the most adverse probability distribution that maximizes the purchasing cost. Since the probability distribution values of the individual discrete scenarios still have uncertainty, the solution is to determine a suitable set of uncertain distributions, limiting the possible values of uncertainty variable that can be taken. The form of set $\Omega$ will be introduced in next section.

#### 2.2.2. Comprehensive norm constraint conditions

Within the three-layer two-stage distributionally robust optimization model, it is necessary to determine an uncertainty set such that the obtained probability distribution values are close to the actual operational data. This study constructs an uncertainty set centered around the initial probability distribution, which satisfies the comprehensive norm constraint conditions. The comprehensive norms include the 1-norm and the infinity-norm, with their feasible regions being $\Omega_1$ and $\Omega_\infty$, respectively, as shown in Equations (22) and (23).

$$\Omega_1 = \left\{ \{p_k\} \in R_+^K \middle| \sum_{k=1}^{K} |p_k - p_k^0| \le \theta_1 \right\} \tag{22}$$

$$\Omega_\infty = \left\{ \{p_k\} \in R_+^K \middle| \max_k |p_k - p_k^0| \le \theta_\infty \right\} \tag{23}$$

where $p_k^0$ is the initial probability value for the $k$ scenario obtained from actual operational data. $\theta_1$ and $\theta_\infty$ are the permissible deviation limits for the 1-norm and infinity-norm probabilities, respectively. The scenario probabilities should satisfy the confidence constraint, as shown in Equation (24).

$$\begin{cases} Pr\left\{ \sum_{k=1}^{K} |p_k - p_k^0| \le \theta_1 \right\} \ge 1 - 2Ke^{-\frac{2M\theta_1}{K}} \\ Pr\left\{ \max_k |p_k - p_k^0| \le \theta_\infty \right\} \ge 1 - 2Ke^{-2M\theta_\infty} \end{cases} \tag{24}$$

where $K$ is the number of discrete scenarios and $M$ is the historical data sample size. By setting the right-hand side of Equation (24) to the confidence levels $\alpha_1$ and $\alpha_\infty$ respectively, we can obtain Equation (25):

$$\begin{cases} \theta_1 = \dfrac{K}{2M} \ln\left(\dfrac{2K}{1-\alpha_1}\right) \\ \theta_\infty = \dfrac{1}{2M} \ln\left(\dfrac{2K}{1-\alpha_\infty}\right) \end{cases} \tag{25}$$

By using the integrated norm, the uncertainty set in this study effectively avoids extreme cases. The final uncertainty probability confidence set, under the integrated norm constraint, is presented in Equation (26), providing the foundation for determining the scenario probability distribution values that maximize the expected objective function.

$$\Omega=\left\{\{p_k\}\left|\begin{array}{l} p_k\geq 0, k=1,\ldots,k \\ \sum_{k=1}^{K} p_k=1 \\ \sum_{k=1}^{K}\left|p_k-p_k^0\right|\leq\theta_1 \\ \max_k\left|p_k-p_k^0\right|\leq\theta_\infty \end{array}\right.\right. \tag{26}$$

*2.2.3. Column and constraint generation algorithm*

To facilitate the solution, the original problem is divided into a master problem and a subproblem, and the column and constraint generation (CCG) algorithm is used to solve them. The master problem is to find the optimal solution under a known finite set of adverse probability distributions, and the form of the master problem is as follows:

$$\min_{x\in X, y_k^m\in Y(x,\xi_k), L} a^T x+L \tag{27}$$

$$s.t.\begin{cases} Ax\leq c \\ Bx+Cy_k^m\leq d\forall k,\forall m=1,\ldots,n \\ \xi_k x+Dy_k^m\leq e\forall k,\forall m=1,\ldots,n \\ Ey_k^m\leq f\forall k,\forall m=1,\ldots,n \\ Fy_k^m=g\forall k,\forall m=1,\ldots,n \\ L\geq\sum_{k=1}^{K} p_k^m\cdot(b^T y_k^m)\forall k,\forall m=1,\ldots,n \end{cases} \tag{28}$$

where $m$ denotes the number of iterations. Given the first-stage variables $x^*$, the purpose of the subproblem is to obtain the most adverse probability distribution $\{p_k\}$. The form of the subproblem is shown in equation (29). Since the minimization problems $\left\{b^T y_k\right\}$ for each scenario are independent, they can be solved separately to accelerate the solution speed.

$$L(x^*)=\max_{\{p_k\}\in\Omega}\sum_{k=1}^{K}\left(p_k\cdot\min_{y_k\in Y(x^*,\xi_k)}\left(b^T y_k\right)\right) \tag{29}$$

The algorithmic procedure for solving the two-stage distributionally robust optimization model using the CCG algorithm is as follows:

Step 1: Set the lower bound ($LB$) to 0, the upper bound ($UB$) to $+\infty$, and the number of iterations $m$ to 1;

Step 2: Solve the master problem to obtain the optimal solution ($x^*$, $L^*$). Update the lower bound according to $LB=\max\left\{LB, a^T x^*+L^*\right\}$;

Step 3: With $x^*$ determined, solve the subproblem to obtain the optimal solution $\left\{p_k^*\right\}$ and the optimal function value $L(x^*)$. Update the upper bound according to $UB=\min\left\{UB, a^T x^*+L(x^*)\right\}$;

Step 4: If $(UB-LB)\leq\varepsilon$, the algorithm terminates and returns the optimal solution $x^*$. Otherwise, update the most adverse probability distribution for the master problem according to $p_k^{m+1}=p_k^*$;

Step 5: Set $m=m+1$ and return to Step 2.

## 3. Research scope and data

### 3.1. Research scope

We select China as the research subject given its vast territory, large number of renewable energy bases, and extensive inter-regional electricity transmission. Within China, 210 sites are selected across five northern provinces that currently serve as the country's main electricity-exporting regions: Inner Mongolia (NM), Ningxia (NX), Qinghai (QH), Gansu (GS), and Xinjiang (XJ). The selection of these specific sites follows three criteria. First, each site corresponds to a wind or solar power base that has already been built or is under construction as of 2023, which ensures that the locations are realistic for large-scale renewable development. Second, the sites are confined to provinces with confirmed inter-regional UHV transmission projects, so that the "power export base" setting in our model is consistent with actual planning practice. Third, the sample is designed to cover the heterogeneous resource conditions of the region, spanning wind-dominant, solar-dominant, and wind-solar complementary sites, so that the analysis captures the full range of resource endowments rather than a single resource type. The spatial distribution and actual capacities of the selected sites are shown in Fig. 2. We note that this study does not use the real installed capacities of these bases; instead, we draw only on their geographic coordinates to obtain resource data and recalculate the cost-optimal capacity configuration. Among the 210 sites, 86 are located in Inner Mongolia, 55 in Xinjiang, 34 in Gansu, 23 in Qinghai, and 12 in Ningxia, which broadly reflects the relative scale of renewable development across the five provinces.

In the basic optimization model, each of the 210 sites is treated as an independent electricity-exporting region supplying power to a common virtual importing region. We deliberately abstract away from the actual transmission directions of specific projects, in order to focus on the influence of resource characteristics rather than the idiosyncrasies of individual corridors. Resource data for each site cover the 8,760 h of the year 2023. In the distributionally robust optimization model, we select one representative site from each of the five provinces. The criterion for representativeness is that the site's annual capacity factor closely matches the provincial average, so that its long-term resource profile can reasonably proxy the province as a whole. The distributionally robust model therefore includes five sites, but extends the study period to ten years from 2014 to 2023, covering 87,600 h (with one day removed in each leap year).

### 3.2. Data

Table 1 reports the key technical and economic parameters used in this study, together with their sources. The main technologies considered, namely wind power, solar PV, energy storage, and transmission lines, are characterized by both one-time investment costs and annual fixed operation and maintenance costs. The values in Table 1 already incorporate these cost components and have been converted into annuities using a 7% discount rate, following Dowling et al. [28]. We adopt this discount rate because it is widely used in capacity-expansion modeling of power systems and falls within the range commonly applied to long-term energy infrastructure investment in China.

The costs of these technologies are assumed to be uniform across regions, so that regional differences in the optimization results arise solely from variations in natural resource conditions. This assumption is consistent with the goal of isolating the role of resource endowments, and is reasonable in the Chinese context, where equipment markets and engineering costs for wind, solar, and storage are highly integrated nationally. Because the study does not target a specific importing region, the renewable export bases are assumed to deliver power to a load center located 1,500 km away. Transmission costs are accordingly evaluated based on an ± 800 kV ultra-high-voltage direct current (UHVDC) line of 1,500 km, which is the dominant configuration for long-distance, large-capacity inter-regional transmission in China.

For the electricity demand of the importing region, we assume a total annual demand of 1 TWh. This figure affects only the absolute scale of the optimal capacity but not the relative proportions of different technologies, which are the primary focus of this study. The hourly load profile is reconstructed from the typical daily load curve and the daily maximum and minimum loads of Henan Province published by the National Development and Reform Commission [29]. Henan is chosen as the demand benchmark because it is one of the largest electricity-receiving provinces in China and a typical destination of UHVDC corridors. The local electricity price faced by the importing region is shown in Fig. 3. Based on the current time-of-use pricing mechanism, daily

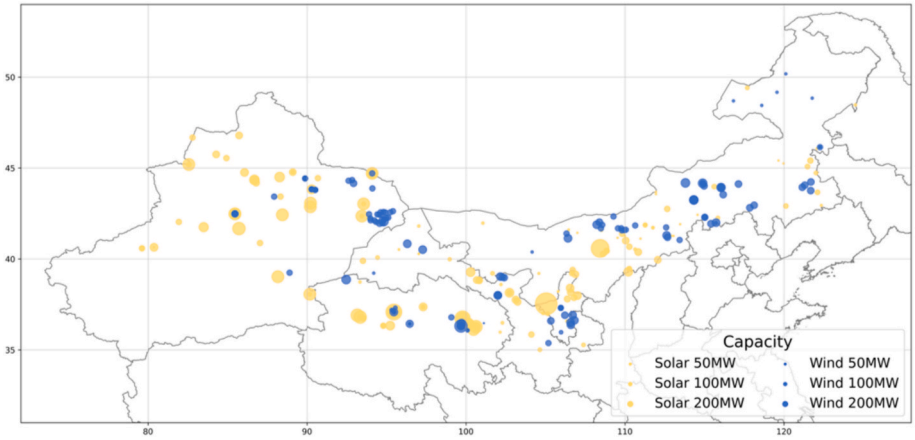


**Fig. 2.** Actual wind and solar PV plants and their capacity.

**Table 1**
Key technical parameters.

| Parameter | Value | Unit | Sources |
|---|---|---|---|
| Charging efficiency | 95 | % | Cole and Karmakar [32] |
| Discharging efficiency | 95 | % | Cole and Karmakar [32] |
| Battery storage hours | 4 | h | Cole and Karmakar [32] |
| Annuity cost of wind farms | 523 | CNY/kW/a | Chen et al. [33], CREEI [34] |
| Annuity cost of solar plants | 352 | CNY/kW/a | Chen et al. [33], CREEI [34] |
| Annuity cost of transmission line | 227 | CNY/kW/a | Yi et al. [35], Zhang and Chen [36] |
| Annuity cost of battery | 172 | CNY/kWh/a | Zhuo et al. [37], Cole and Karmakar [32] |

prices are divided into peak, high, standard, and off-peak periods, at 0.72, 0.6, 0.4, and 0.2 CNY/kWh, respectively, with these rates varying by month.

Hourly capacity factor data for wind and solar power are obtained from the Renewables.ninja platform. The underlying weather datasets and the methodology for converting them into capacity factors are documented in Pfenninger and Staffell [30] and Staffell and Pfenninger [31]; we use the platform's default turbine and PV technology specifications, which are appropriate for utility-scale projects. Fig. 4 illustrates the distribution of capacity factors across the 210 sites in different seasons of 2023, and Table 2 reports the annual average capacity factors over the past decade for the five sites used in the distributionally robust optimization.

## 4. Results of basic optimization model

### 4.1. Capacity configuration

Fig. 5 uses the ratio of the wind power capacity factor to the solar PV capacity factor (denoted as wind-to-solar) as a key indicator of resource endowment, and examines its effect on the installed capacities of wind power, solar PV, and energy storage. Panel A of Fig. 5 shows that the installed capacities of wind and solar PV are strongly positively correlated with their respective resource conditions, and that in most cases the two technologies coexist. This co-deployment holds even when the levelized cost of electricity (LCOE) of one technology is markedly lower than that of the other, which highlights the complementarity between the two resources. When the wind-to-solar ratio reaches about 1.5, the installed capacities of wind and solar PV are roughly 1:1, providing a useful reference for regions to determine their renewable mix based on local resource conditions. Although the capacity factor of solar PV is generally lower than that of wind power, the peak values of the blue and yellow trend lines in the figure are not markedly different, implying that wind generation from wind-rich regions is in fact higher than solar generation from solar-rich regions. The underlying reason is that solar PV exhibits stronger intra-day fluctuations than wind, so wind power achieves a higher average utilization rate of the transmission channel. As a result, wind power holds a structural advantage in delivering electricity from renewable export bases. This finding contrasts with studies focused on distributed PV in load-center regions (e.g., [12]), where storage co-deployment is dominated by daily self-consumption logic rather than transmission utilization, indicating that the optimization logic for export bases is fundamentally different.

Panel B of Fig. 5 shows that the installed capacity of energy storage exhibits an inverted U-shaped relationship with the wind-to-solar ratio. The right half of this relationship is comparatively easy to interpret, since solar PV depends more heavily on storage than wind power. In regions where wind resources dominate, storage demand remains very low, and in some cases falls to zero. This indicates that at current storage prices, not all renewable energy bases require storage, and that the key determinant of storage necessity is the wind-to-solar capacity factor ratio within the base. Wind power undergoes smaller intra-day output fluctuations than solar PV and is therefore inherently less reliant on storage. However, when combined with solar PV, wind power raises the overall output level: for a given solar PV capacity, the presence of wind power produces a higher peak output, which in turn increases the need for storage. This mechanism explains the trend observed in the far-left portion of the figure.

At these specific data points, wind resources are typically very poor, leading to a very low wind-to-solar ratio and correspondingly small wind capacity. Solar PV resources, by contrast, are nearly fully exploited, and further expanding a single-source configuration would require additional transmission or storage. The economic feasibility of such an expansion may even fall below that of direct electricity purchases in the importing region. Consequently, solar PV capacity remains largely flat, producing the seemingly unusual phenomenon in which the wind-to-solar ratio and storage demand move in the same direction. This yields an interesting and policy-relevant insight: in export bases with complementary wind and solar resources, better wind resources reduce the need for storage; yet when wind resources are extremely poor, storage demand does not reach its highest level. The peak storage demand instead occurs in regions where wind resources are relatively weak but still competitive. For project developers and provincial planners, this implies that uniform storage mandates applied across all renewable bases are likely to be economically inefficient, and that storage allocation should be tailored to the local wind-to-solar ratio.

Fig. 6 presents storage and transmission capacity under different wind and solar resource conditions. Panel A of Fig. 6 reinforces the preceding conclusion: at the same wind power level, the more abundant

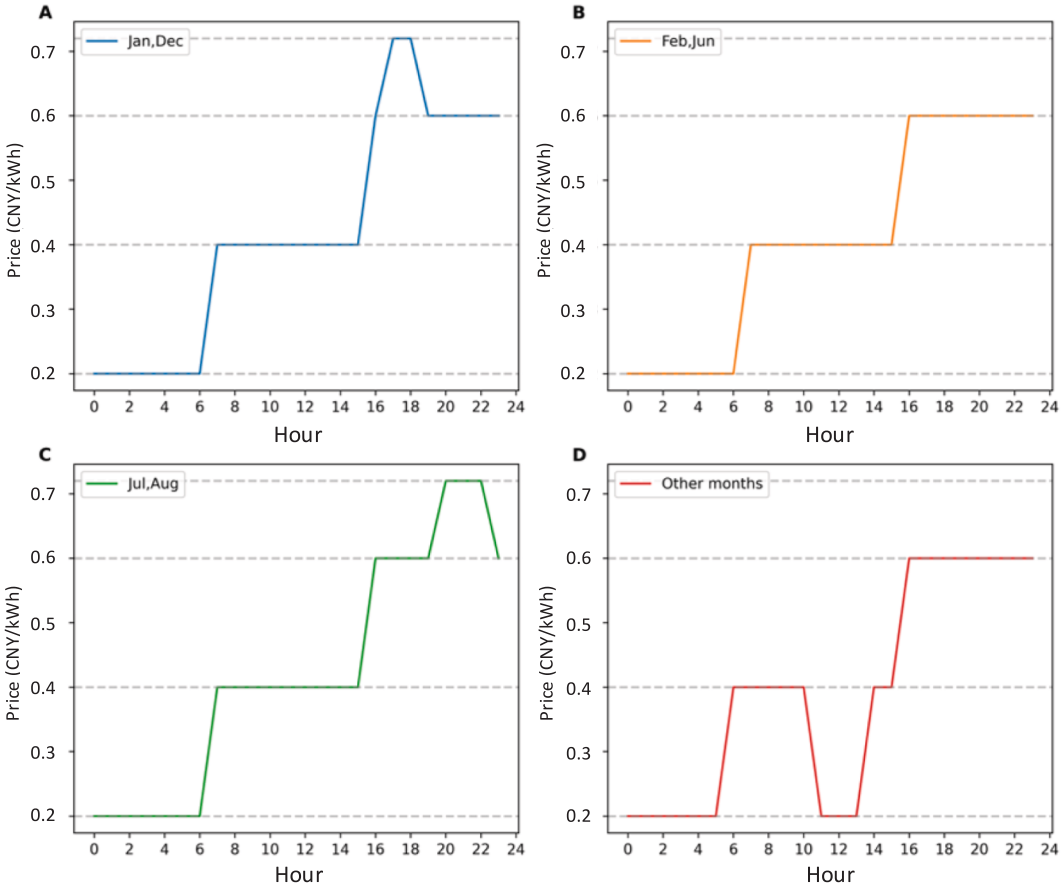


**Fig. 3.** Parameter setting of time-of-use pricing.

the solar resources, the greater the required storage capacity; whereas at the same solar power level, weaker wind resources do not necessarily imply higher storage demand. The points with the highest storage requirements are concentrated in the bottom-right of the figure, where solar resources are abundant and wind resources are relatively weak. By contrast, the points with the lowest storage requirements are concentrated in the upper part of the figure, where wind resources are most abundant; in this region the relationship with solar resource levels is weak, because the advantage of wind power dominates.

Panel B of Fig. 6 illustrates the influence of resource conditions on transmission line capacity. The variation in transmission capacity is comparatively narrow, ranging from 111.64 MW to 129.95 MW, but this should be interpreted in light of the load curve, whose peak reaches 194.12 MW. A transmission capacity of 129.95 MW exceeds the load 81.5% of the time, whereas 111.64 MW exceeds the load only 55% of the time, so the apparently small numerical range in fact corresponds to a substantial difference in supply adequacy. Renewable bases in wind-rich areas generally require larger transmission capacities, while the relationship with solar resource conditions is weak. This is because pairing solar PV with storage is more economical than expanding transmission: on one hand, larger transmission capacity reduces corridor utilization; on the other, midday electricity prices in the importing region are relatively low, limiting the marginal revenue that additional transmission capacity could generate.

### 4.2. Provincial characteristics

The five provinces selected in this study display markedly different resource profiles. The best wind resources are found in Inner Mongolia, the best solar resources in Qinghai, and the other three provinces exhibit relatively balanced wind and solar conditions. Fig. 7 reports provincial-level averages of capacity, generation, and cost. The optimal wind-to-solar capacity ratios for Inner Mongolia, Ningxia, Gansu, Xinjiang, and Qinghai are 2.13, 0.93, 0.75, 0.51, and 0.44, respectively. Gansu, which has the most balanced resources, exhibits an almost 1:1 wind-to-solar generation ratio. Correspondingly, renewable bases in Inner Mongolia require the least storage, while those in Qinghai require the most; the remaining three provinces show broadly similar optimal storage capacities, averaging roughly 18% to 28% of total installed wind and solar capacity. Throughout this paper, storage capacity is measured in MW (conversion capacity) rather than in MWh (energy capacity), and this convention is applied consistently in the subsequent sections. In provinces with abundant wind resources, the generation of outbound bases can meet a larger share of demand in the importing region, thereby reducing local electricity purchases. As shown in Panel B of Fig. 7, the average electricity supply rate reaches 65.56% in Inner Mongolia but only 44.93% in Qinghai. Across all 210 sites, the highest supply rate is 72.37%, in Urat Middle Banner (Inner Mongolia), and the lowest is 31.19%, in Hutubi County (Xinjiang).

From a cost perspective, wind-rich regions also have the lowest electricity costs. As a power-exporting base, Inner Mongolia delivers electricity to the importing region at an average cost of just 0.305 CNY/kWh, whereas the other provinces range from 0.348 to 0.356 CNY/kWh. Considering only the supply cost of the outbound base (including storage and transmission), Inner Mongolia falls as low as 0.240 CNY/kWh, while the other provinces range from 0.330 to 0.379 CNY/kWh. Although the LCOE of solar PV is not high, the additional storage requirement and the higher per-unit transmission cost allocation jointly limit its economic competitiveness for long-distance export. Average transmission costs across provinces are similar, but lower PV generation leads to higher cost allocation per unit of electricity delivered. As a result, in renewable export bases, the inherent characteristics of solar PV render it less

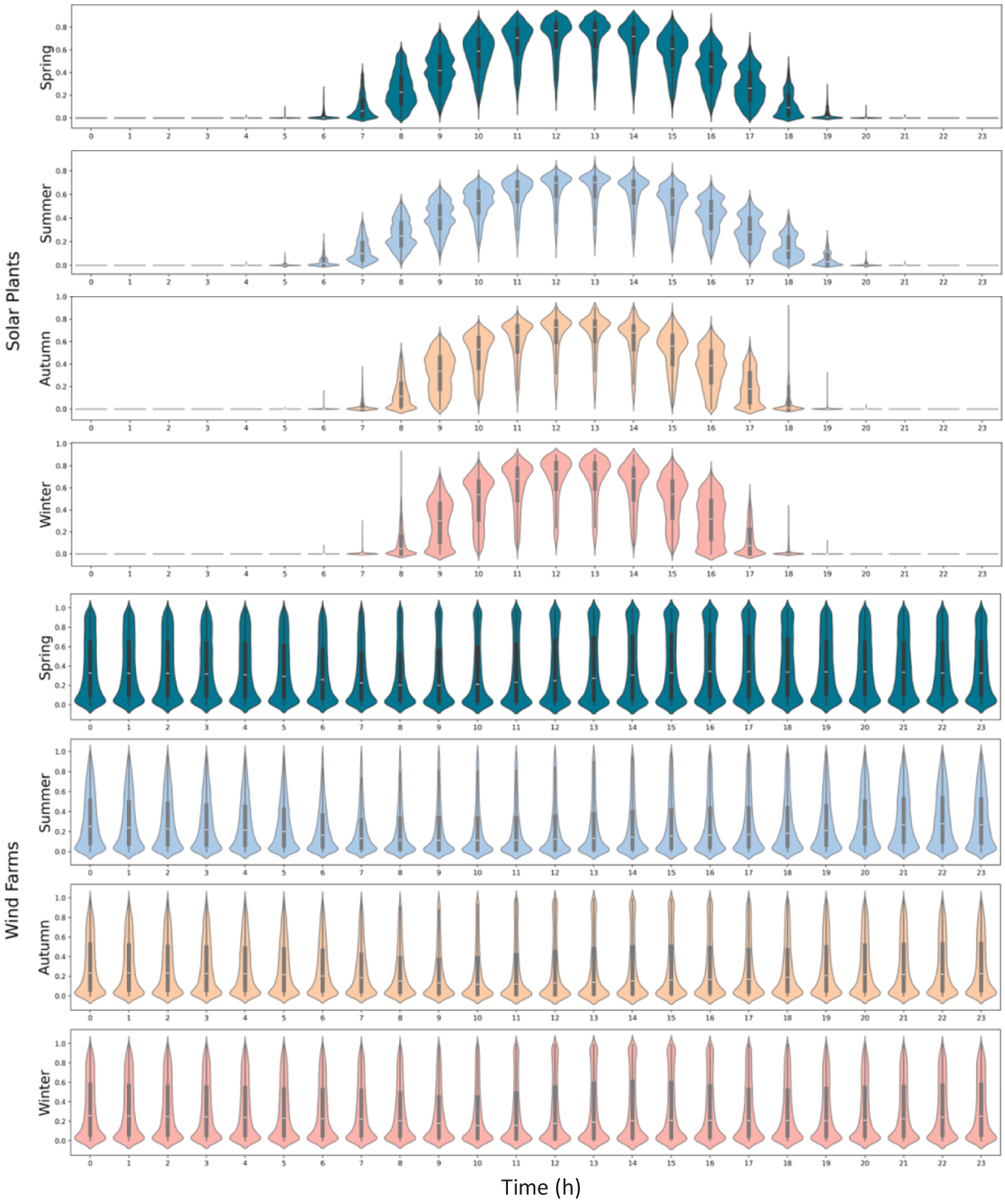


**Fig. 4.** Hourly distribution characteristics of wind and solar PV capacity factor in 2023.

economical than wind power under otherwise comparable conditions. These provincial-level differences are also consistent with observed practice: the four UHVDC corridors already operating out of Inner Mongolia have systematically shown higher utilization hours than the corridors originating from Qinghai and Xinjiang, which supports the validity of our cost-ranking results.

### *4.3. Single renewable energy cases*

To assess the role of wind-solar complementarity in storage demand, we re-optimize two counterfactual cases that exclude either wind or solar power; the results are reported in Fig. 8. In the single-PV case, there is a clear positive correlation between the solar PV capacity factor and the required storage capacity, and the storage ratio per unit of PV capacity rises sharply in resource-rich regions. For example, at a capacity factor of 0.19 the storage ratio is about 4.9% of PV capacity; at 0.21 it rises to 13.3%; and at 0.24 it reaches 26.3%. This implies that the optimal storage-to-PV ratio should vary substantially across regions. If bundling with coal-fired power is not considered, China's current PV storage mandates are broadly reasonable in magnitude, though the uniform ratios applied across regions are clearly inconsistent with the regional differentiation implied by our results.

**Table 2**
Average wind and solar PV capacity factors by province over the years.

| Year | Average solar PV capacity factor | | | | | Average wind capacity factor | | | | |
|---|---|---|---|---|---|---|---|---|---|---|
| | QH | XJ | GS | NX | NM | QH | XJ | GS | NX | NM |
| 2014 | 0.235 | 0.209 | 0.206 | 0.200 | 0.189 | 0.190 | 0.196 | 0.231 | 0.262 | 0.326 |
| 2015 | 0.239 | 0.205 | 0.204 | 0.199 | 0.189 | 0.222 | 0.239 | 0.257 | 0.268 | 0.349 |
| 2016 | 0.236 | 0.200 | 0.202 | 0.202 | 0.193 | 0.244 | 0.219 | 0.237 | 0.275 | 0.364 |
| 2017 | 0.234 | 0.201 | 0.203 | 0.200 | 0.196 | 0.205 | 0.231 | 0.247 | 0.258 | 0.395 |
| 2018 | 0.231 | 0.207 | 0.201 | 0.199 | 0.196 | 0.212 | 0.232 | 0.238 | 0.281 | 0.396 |
| 2019 | 0.230 | 0.203 | 0.204 | 0.198 | 0.197 | 0.201 | 0.243 | 0.236 | 0.276 | 0.399 |
| 2020 | 0.234 | 0.211 | 0.208 | 0.203 | 0.190 | 0.172 | 0.221 | 0.225 | 0.232 | 0.411 |
| 2021 | 0.234 | 0.204 | 0.210 | 0.203 | 0.187 | 0.200 | 0.221 | 0.255 | 0.295 | 0.411 |
| 2022 | 0.233 | 0.206 | 0.202 | 0.202 | 0.193 | 0.204 | 0.222 | 0.219 | 0.253 | 0.403 |
| 2023 | 0.237 | 0.206 | 0.207 | 0.203 | 0.196 | 0.206 | 0.237 | 0.254 | 0.284 | 0.401 |

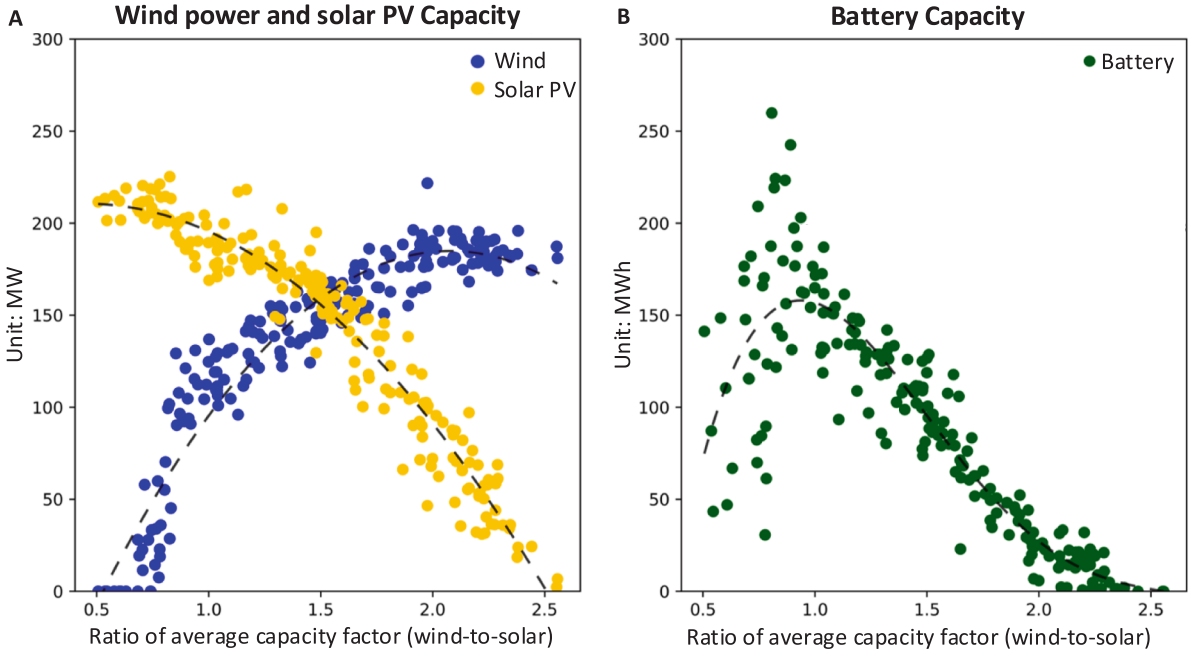


**Fig. 5.** Capacity of solar PV, wind power, and battery storage under varying wind-to-solar capacity factor ratios.

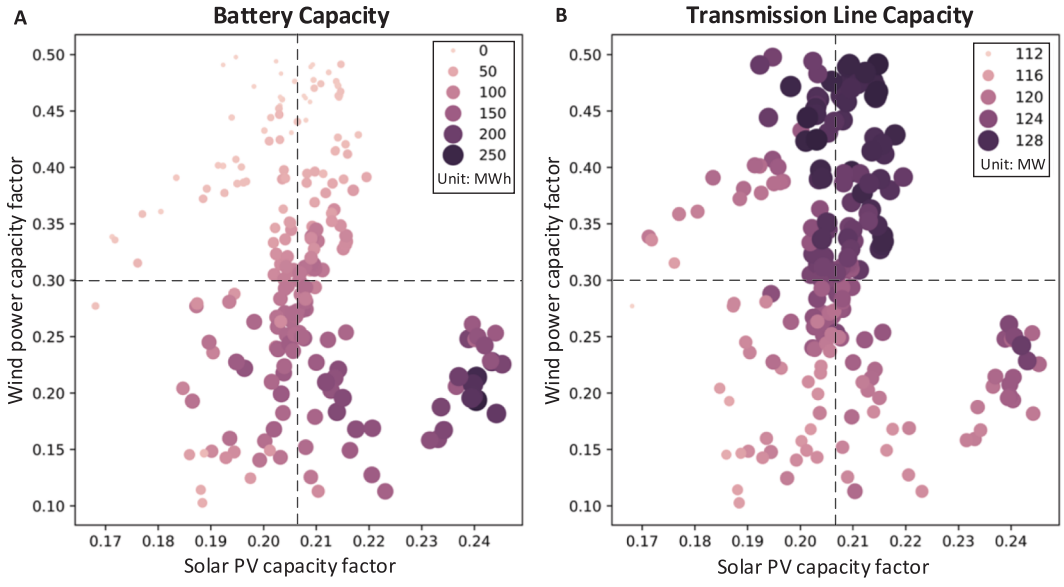


**Fig. 6.** Capacity of battery storage and transmission lines under varying resource conditions.

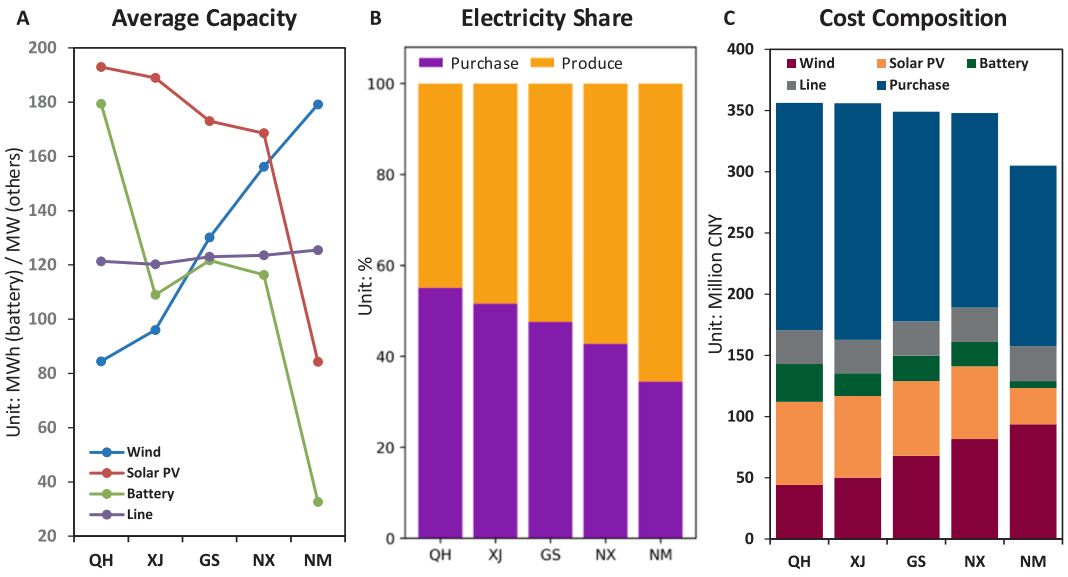


**Fig. 7.** Provincial average level.

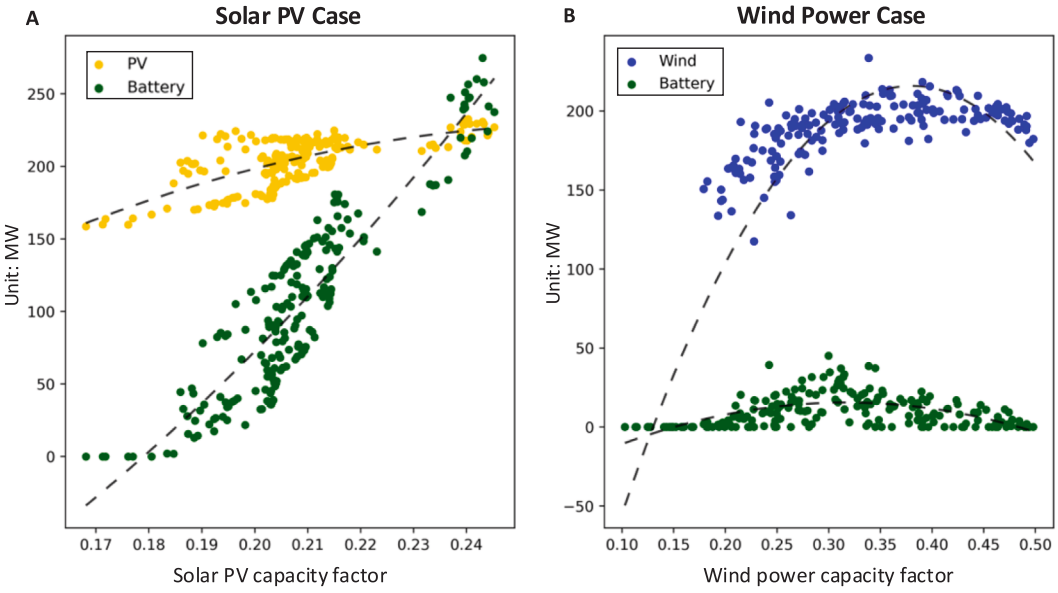


**Fig. 8.** Capacity configuration in standalone power source cases.

In the single-wind case, by contrast, very little storage is required regardless of wind resource conditions, and some locations require none at all. The highest storage ratio does not exceed 6% of wind capacity, and 88% of locations have a storage ratio below 3%. This stands in sharp contrast to current practice in China, where many provinces require wind power storage ratios that are equal to or even higher than those for solar PV, an arrangement that is difficult to justify on economic grounds. In addition, comparing the minimum cost of the single-wind or single-PV case with the cost under wind-solar complementarity at each site, we find that abandoning complementarity raises the overall electricity cost by 3.6% on average. The effect is particularly pronounced in Ningxia, Gansu, and Xinjiang, where wind and solar resources are relatively balanced, which underscores the practical importance of adopting a complementary configuration in new renewable bases. Taken together, these results offer two concrete policy implications: storage allocation rules should be differentiated by both resource type and resource quality rather than imposed as uniform ratios, and the planning of new renewable export bases should explicitly exploit wind-solar complementarity rather than treat the two resources in isolation.

## 5. Results of distributionally robust optimization model

### 5.1. Solution of the DRO model

In the DRO model, the confidence levels $\alpha_1$ and $\alpha_\infty$ are set at 0.99. The number of discrete scenarios $K$ is 10, with each scenario corresponding to one complete calendar year of hourly capacity factor data (8,760 h) from 2014 to 2023. $K$ is therefore not a tunable hyperparameter but is determined by the number of distinct resource years in the data window; each scenario is a high-fidelity hourly trajectory rather than an annual average, so the intra-day fluctuations, seasonality, wind-solar correlation, and extreme periods of each year are preserved as inputs to the optimization. The initial probability of each discrete scenario is set to 0.1. This study conducts numerical experiments on five representative sites, each corresponding to one of the five selected provinces. The CCG algorithm is employed to solve the DRO problem. As

shown in Table 3, the discrepancy between the master problem and the subproblem falls below the accuracy threshold after two iterations for all five sites, leading to the termination of the iterative process. The rapid convergence reflects the well-posed master-subproblem structure under our scenario formulation, rather than the triviality of the worst-case adjustment; as shown in Section 5.2, the resulting robust configurations differ from the deterministic solution in capacity-level, directionally consistent ways across all sites. This demonstrates that the CCG algorithm is effective in solving the two-stage DRO model proposed here.

### 5.2. The impact of resource uncertainty

After accounting for the uncertainty of wind and solar resources, the installed capacity of wind power generally decreases by 1% to 7%, while the installed capacity of solar PV rises only modestly, as shown in Fig. 9. The underlying reason is that wind power exhibits substantially higher inter-annual uncertainty than solar PV. As the data window lengthens, the probability of encountering years with poor resource conditions rises, and the DRO model places greater weight on such adverse scenarios, adjusting the optimal configuration accordingly. In principle, resource uncertainty affects both technologies; however, because solar PV is less exposed to year-on-year fluctuations, part of the wind capacity is replaced by solar PV, and a further share is substituted by local electricity purchases in the importing region. As a result, the optimal solar PV capacity does not decline but instead increases slightly. Accounting for resource uncertainty therefore lowers the wind-to-solar ratio of renewable energy bases, with the effect most pronounced in wind-rich regions.

Building on this finding, we can use Fig. 6 to assess how these shifts affect storage and transmission capacity. Effectively, accounting for uncertainty implies that the realized resource conditions for solar PV are slightly weaker, while those for wind power are considerably weaker, than in the deterministic case. For energy storage, no clear directional pattern emerges: solar conditions are the primary driver of storage demand, but the influence of weakened wind conditions is ambiguous, so the direction of change is indeterminate and the magnitude of variation is small. Nevertheless, since the reduction in wind generation lowers the overall outbound electricity from renewable bases, the required storage capacity per unit of transmitted electricity in fact rises. Overall, accounting for resource uncertainty leads renewable bases to exhibit a consistent pattern of reduced wind capacity, increased solar PV capacity, essentially stable storage capacity, and reduced transmission capacity, though the magnitude of these adjustments varies across locations.

Fig. 10 illustrates the corresponding cost variations. Given the structure of the DRO model, whose second-stage objective is to maximize cost under the worst-case probability distribution, the robust solution naturally yields higher costs than the basic model, which considers only a single deterministic scenario. The more a region relies on wind resources, the larger the cost increase. For example, the unit electricity cost in the importing region supplied by Inner Mongolia rises by approximately 3.3%, whereas in Qinghai the increase is only 0.9%. From a cost perspective, accounting for resource uncertainty makes the importing region more dependent on local electricity purchases, which are considerably more expensive than the supply cost of renewable energy bases.

**Table 3**
Results of CCG algorithm.

| Location | Iteration | Upper bound (Million CNY) | Lower bound (Million CNY) |
|---|---|---|---|
| QH | 1 | 365.432 | 364.077 |
| | 2 | 365.417 | 365.417 |
| XJ | 1 | 366.033 | 364.977 |
| | 2 | 366.030 | 366.030 |
| GS | 1 | 359.866 | 358.259 |
| | 2 | 359.860 | 359.860 |
| NX | 1 | 354.000 | 352.017 |
| | 2 | 353.986 | 353.986 |
| NM | 1 | 316.725 | 313.578 |
| | 2 | 316.715 | 316.715 |

### 5.3. Comparison with stochastic and robust optimization benchmarks

To further substantiate the methodological positioning of the DRO framework, we benchmark it against two alternative uncertainty-handling formulations: a stochastic optimization (SO) model and a robust optimization (RO) model. All three models share an identical optimization framework, constraints, and decision variables, and differ only in how the ten historical resource years are processed. In the SO model, each of the ten annual scenarios is assigned an equal probability of 0.1, and the objective is to minimize the expected total cost. In the RO model, deterministic optimization is performed independently for each of the ten historical years, and the year that yields the highest optimal cost is identified as the worst-case scenario for that site; the capacity configuration optimized against this worst-case year is then taken as the RO solution. The DRO model lies between these two extremes, optimizing against the worst-case probability distribution within a constructed ambiguity set, as described in Section 2. Table 4 reports the resulting capacity configurations and unit electricity costs for all five sites.

Two patterns emerge from the comparison. First, DRO consistently lies between SO and RO across all metrics and all sites, which is the defining methodological property of this formulation. Wind capacity decreases monotonically from SO to DRO to RO, while solar PV capacity, storage capacity, and total cost rise monotonically along the same direction. For example, at Qinghai, wind capacity falls from 95.63 MW (SO) to 92.35 MW (DRO) and further to 54.55 MW (RO), while solar PV capacity rises from 188.87 MW to 190.50 MW and then to 198.02 MW. Similar orderings hold for the other four sites. Second, the gap between DRO and RO is substantially larger than the gap between DRO and SO, indicating that SO underestimates the risk of adverse resource years while RO overcompensates by anchoring on a single extreme year. Across the five sites, the total cost of RO exceeds that of DRO by between 1.3% (XJ) and 6.0% (NM), whereas DRO exceeds SO by only 0.3% (XJ) to 1.0% (NM). This asymmetry confirms that DRO provides cost-effective robustness without paying the full conservatism premium of RO.

Taken together, these comparisons show that the DRO framework adopted here provides a balanced trade-off between the expected-cost efficiency of SO and the worst-case conservatism of RO, and is therefore methodologically appropriate for long-term renewable capacity planning under sample-limited resource uncertainty. The full DRO formulation also retains a meaningful informational advantage over the deterministic models: it exploits the entire ten-year historical record while maintaining hedging capability, rather than either over-trusting the empirical distribution (SO) or discarding all but the worst year (RO).

## 6. Conclusions

This study develops a basic optimization model and a distributionally robust optimization model for the Wind-Solar-Storage-Transmission (WSST) system to investigate capacity allocation under different resource conditions. The analysis covers 210 sites across five provinces in northern China, and yields the following conclusions.

The installed capacities of wind and solar power are strongly positively correlated with their respective resource conditions, yet the two technologies exhibit both competition and a notable degree of complementarity. Because solar PV undergoes larger intra-day fluctuations than wind, transmitting wind power yields a higher average utilization rate of the transmission corridor. Under equivalent resource conditions, wind power therefore enjoys a structural advantage for export-oriented

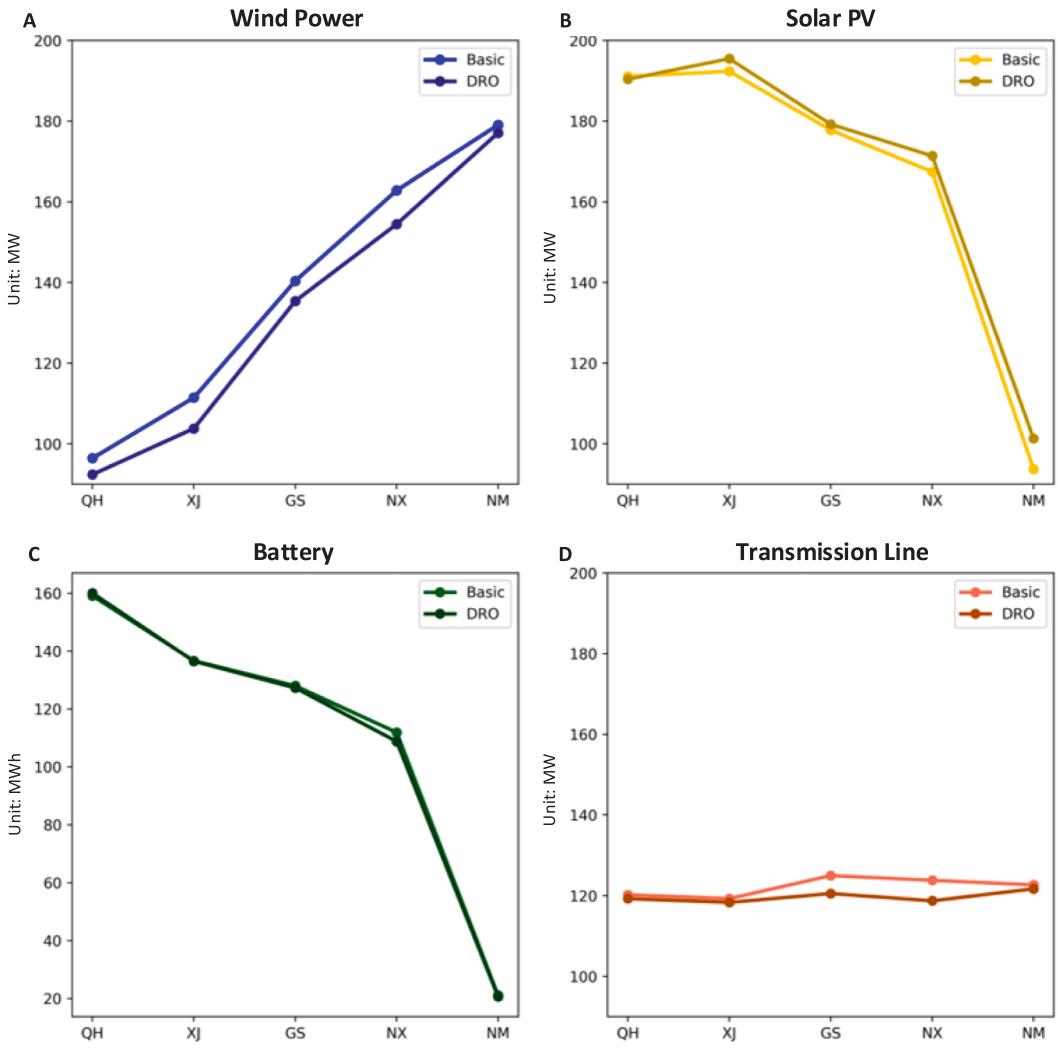


**Fig. 9.** Capacity configuration comparison between two models.

renewable bases. When the wind-to-solar capacity factor ratio reaches about 1.5, the installed capacities of wind and solar power are roughly equal. Even when the resource condition of one technology is markedly better than that of the other, the two sources are very likely to coexist. Exploiting this complementarity reduces the average electricity cost by 3.6% relative to single-source configurations, and is especially valuable in Ningxia, Gansu, and Xinjiang, where wind and solar resources are relatively balanced and complementary configurations of renewable bases are clearly more beneficial.

At current energy storage prices, not all renewable bases need to be equipped with storage, and the key determinant is the wind-to-solar capacity factor ratio within the base. Compared with wind power, solar PV depends far more heavily on storage. In single-source cases, the solar capacity factor is strongly positively correlated with the level of installed storage, and the required storage capacity per unit of installed PV rises sharply in areas with better solar resources. Wind power, by contrast, requires only minimal storage regardless of resource conditions, and some regions require none at all. In many parts of China, however, wind power is mandated to carry storage ratios equal to or higher than those imposed on solar PV, which is difficult to justify on economic grounds. Under wind-solar complementarity, the installed storage capacity follows an inverted U-shaped relationship with the wind-to-solar capacity factor ratio: better wind resources reduce storage demand, but peak storage demand does not occur where wind resources are weakest. Rather, peak demand arises where wind resources are relatively weak but still competitive. At the provincial level, renewable bases in Inner Mongolia require the least storage, while those in Qinghai sit at the opposite extreme; the optimal storage capacities of the other three provinces are broadly similar, averaging about 18% to 28% of total installed wind and solar capacity.

The influence of resource conditions on transmission line capacity is comparatively limited, primarily because the load concentration periods span only a narrow range. In general, renewable bases in wind-rich regions require larger transmission capacities, while their relationship with solar resource conditions is much weaker.

The uncertainty of wind power is markedly higher than that of solar PV. When resource uncertainty is taken into account, the installed capacity of wind power generally declines by 1% to 7%, while that of solar PV rises slightly, though the increase is modest. Overall, accounting for resource uncertainty leads renewable export bases to exhibit a consistent pattern of reduced wind capacity, increased solar PV capacity, essentially unchanged storage, and reduced transmission capacity. Consequently, when the optimal configuration of a WSST system is estimated using only recent deterministic capacity factors, the resulting allocations should be adjusted accordingly to reflect long-term resource variability.

## CRediT authorship contribution statement

**You Zhou:** Writing – original draft, Visualization, Validation,

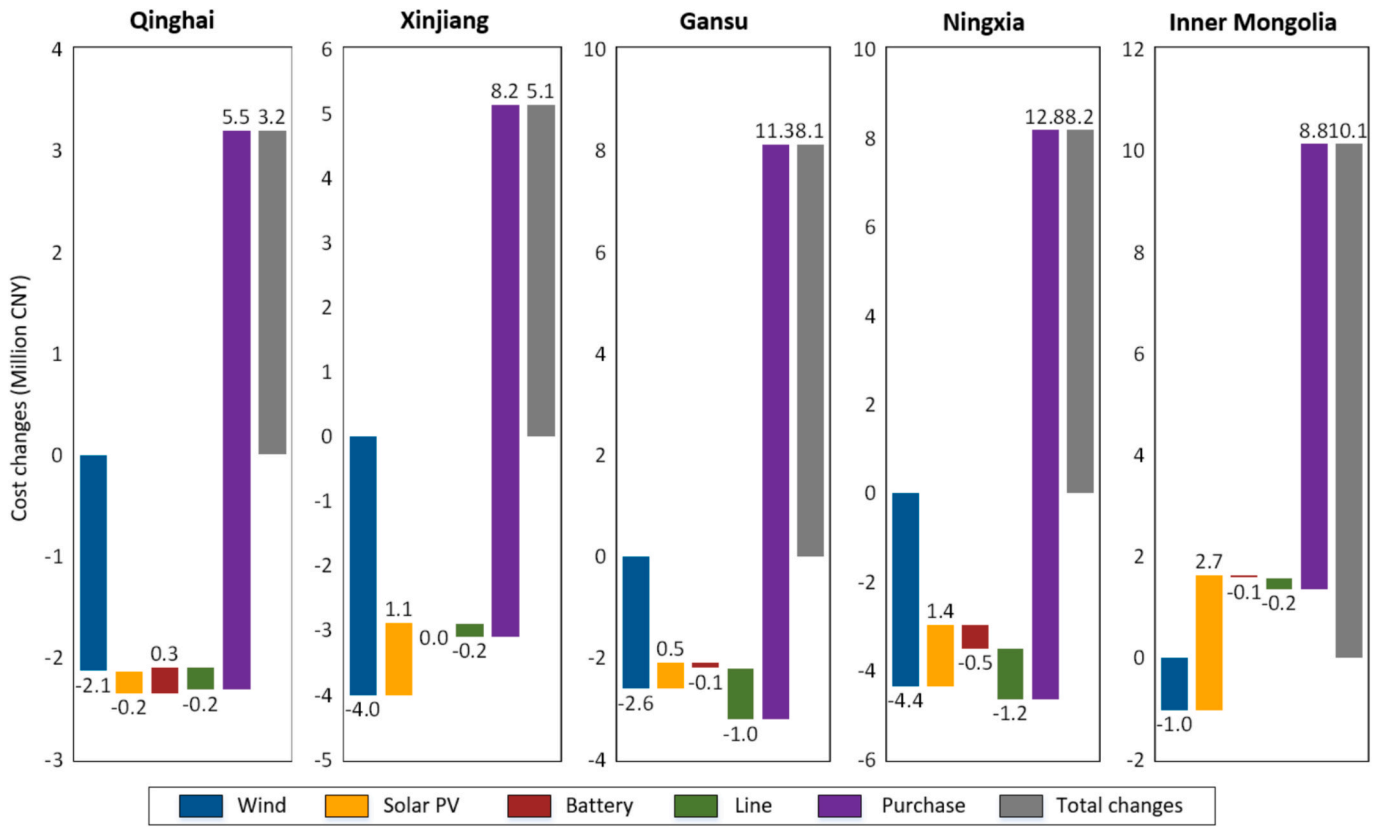


**Fig. 10.** Cost changes in the DRO model compared to the basic model.

**Table 4**
Comparison of capacity configurations across SO, DRO, and RO models.

| Site | Model | Wind (MW) | Solar (MW) | Storage (MWh) | Transmission (MW) | Cost (Million CNY) |
|---|---|---|---|---|---|---|
| QH | SO | 95.63 | 188.87 | 156.28 | 119.39 | 364.077 |
| | DRO | 92.35 | 190.50 | 160.59 | 119.25 | 365.417 |
| | RO | 54.55 | 198.02 | 166.31 | 118.00 | 370.885 |
| XJ | SO | 104.78 | 194.69 | 135.43 | 118.51 | 364.977 |
| | DRO | 103.79 | 195.53 | 136.61 | 118.36 | 366.030 |
| | RO | 78.92 | 212.02 | 182.43 | 117.50 | 370.898 |
| GS | SO | 136.76 | 178.35 | 126.75 | 121.19 | 358.259 |
| | DRO | 135.41 | 179.23 | 127.35 | 120.54 | 359.860 |
| | RO | 131.53 | 185.20 | 130.74 | 118.55 | 364.887 |
| NX | SO | 156.69 | 169.37 | 105.23 | 119.40 | 352.017 |
| | DRO | 154.51 | 171.39 | 108.78 | 118.75 | 353.986 |
| | RO | 137.02 | 179.68 | 122.32 | 115.41 | 367.258 |
| NM | SO | 178.12 | 97.88 | 19.68 | 122.22 | 313.578 |
| | DRO | 177.07 | 101.31 | 20.74 | 121.71 | 316.715 |
| | RO | 172.98 | 131.89 | 37.39 | 122.58 | 335.868 |

Methodology. **Hao He:** Writing – original draft, Methodology, Investigation. **Shaohui Zhang:** Investigation, Data curation, Conceptualization. **Fuwenxin Yu:** Software, Methodology. **Bowen Yi:** Writing – original draft, Supervision, Methodology.

## Declaration of competing interest

The authors declare that they have no known competing financial interests or personal relationships that could have appeared to influence the work reported in this paper.

## Acknowledgement

This work is supported by the Fundamental and Interdisciplinary Disciplines Breakthrough Plan of the Ministry of Education of China under Grant No. JYB2025XDXM904, and the National Natural Science Foundation of China under Grant No.72374018, No.W2412161.

## Data availability

Data will be made available on request.

## References

[1] Wang Y, Wang R, Tanaka K, et al. Accelerating the energy transition towards photovoltaic and wind in China[J]. Nature 2023;619(7971):761–7.
[2] Neuhoff K, Barquin J, Bialek JW, et al. Renewable electric energy integration: quantifying the value of design of markets for international transmission capacity [J]. Energy Econ 2013;40:760–72.
[3] Van Der Weijde AH, Hobbs BF. The economics of planning electricity transmission to accommodate renewables: using two-stage optimisation to evaluate flexibility and the cost of disregarding uncertainty[J]. Energy Econ 2012;34(6):2089–101.
[4] Yi BW, Xu JH, Fan Y. Inter-regional power grid planning up to 2030 in China considering renewable energy development and regional pollutant control: a multi-region bottom-up optimization model[J]. Appl Energy 2016;184:641–58.
[5] Davidson MR, Zhang D, Xiong W, et al. Modelling the potential for wind energy integration on China's coal-heavy electricity grid[J]. Nat Energy 2016;1(7):1–7.
[6] Merrick JH, Bistline JET, Blanford GJ. On representation of energy storage in electricity planning models[J]. Energy Econ 2024;107675.
[7] Frew B, Sergi B, Denholm P, et al. The curtailment paradox in the transition to high solar power systems[J]. Joule 2021;5(5):1143–67.
[8] Xu JH, Yi BW, Fan Y. Economic viability and regulation effects of infrastructure investments for inter-regional electricity transmission and trade in China[J]. Energy Econ 2020;91:104890.
[9] Li LL, Zhang ZY, Sethanan K, et al. Multi-energy synergistic planning of distributed energy supply system: wind-solar-hydrogen coupling energy supply[J]. Renew Energy 2024;237:121769.
[10] Mahdavi S, Hemmati R, Jirdehi MA. Two-level planning for coordination of energy storage systems and wind-solar-diesel units in active distribution networks[J]. Energy 2018;151:954–65.

[11] Wang J, Wen J, Wang J, et al. Coordinated scheduling of wind-solar-hydrogen-battery storage system for techno-economic-environmental optimization of hydrogen production[J]. Energ Conver Manage 2024;314:118695.
[12] Ghanbari K, Maleki A, Ochbelagh DR. Investigating the effect of various types of components in optimal designing of a solar/wind/storage hybrid system[J]. J Storage Mater 2025;110:115273.
[13] Ruggles TH, Virgüez E, Reich N, et al. Planning reliable wind-and solar-based electricity systems[J]. Adv Appl Energy 2024;15:100185.
[14] Carpio LGT, Guimarães FAC. Regional diversification of hydro, wind, and solar generation potential: a mean-variance model to stabilize power fluctuations in the Brazilian integrated electrical energy transmission and distribution system[J]. Renew Energy 2024;121266.
[15] Denholm P, Sioshansi R. The value of compressed air energy storage with wind in transmission-constrained electric power systems[J]. Energy Policy 2009;37(8):3149–58.
[16] Moradi-Sepahvand M, Amraee T. Integrated expansion planning of electric energy generation, transmission, and storage for handling high shares of wind and solar power generation[J]. Appl Energy 2021;298:117137.
[17] Göke L, Kendziorski M, Kemfert C, et al. Accounting for spatiality of renewables and storage in transmission planning[J]. Energy Econ 2022;113:106190.
[18] Artis R, Shivaie M, Weinsier PD. A flexibility-based multi-objective model for contingency-constrained transmission expansion planning incorporating large-scale hydrogen/compressed-air energy storage systems and wind/solar farms[J]. J Storage Mater 2023;70:108086.
[19] Ma C, Liu L. Optimal capacity configuration of hydro-wind-PV hybrid system and its coordinative operation rules considering the UHV transmission and reservoir operation requirements[J]. Renew Energy 2022;198:637–53.
[20] Sun J, Su C, Song J, et al. Capacity planning for large-scale wind-photovoltaic-pumped hydro storage energy bases based on ultra-high voltage direct current power transmission[J]. Energy 2025;135224.
[21] Fan W, Fan Y, Yao X, et al. Enhancing the capability of integrated energy system to handle uncertainty: balancing robustness, economy and low-carbon operation[J]. Energy Convers Manage: X 2025;101334.
[22] Yang H, Liang R, Yuan Y, et al. Distributionally robust optimal dispatch in the power system with high penetration of wind power based on net load fluctuation data[J]. Appl Energy 2022;313:118813.
[23] Han X, Wang Z, Li H, et al. Cooperative game robust optimization control for wind-solar-shared energy storage integrated system based on dual-settlement mode and multiple uncertainties[J]. Appl Energy 2025;378:124799.
[24] Hua L, Junjie X, Xiang G, et al. Scenario-based stochastic optimization on the variability of solar and wind for component sizing of integrated energy systems[J]. Renew Energy 2024;237:121543.
[25] Kang J, Wu Z, Ng TS, et al. A stochastic-robust optimization model for inter-regional power system planning[J]. Eur J Oper Res 2023;310(3):1234–48.
[26] Wiesemann W, Kuhn D, Sim M. Distributionally robust convex optimization[J]. Oper Res 2014;62(6):1358–76.
[27] Xiao G, Zhang M, Huang W, et al. A data-driven hybrid robust optimization approach for microgrid operators in the energy reserve market considering different wind power producers' strategies[J]. Appl Energy 2025;386:125564.
[28] Dowling JA, Rinaldi KZ, Ruggles TH, et al. Role of long-duration energy storage in variable renewable electricity systems[J]. Joule 2020;4(9):1907–28.
[29] NRDC (National Development and Reform Commission). Notice on the signing of medium and long-term electric power contracts in 2020[EB]. 2019. (in Chinese).
[30] Pfenninger S, Staffell I. Long-term patterns of European PV output using 30 years of validated hourly reanalysis and satellite data[J]. Energy 2016;114:1251–65.
[31] Staffell I, Pfenninger S. Using bias-corrected reanalysis to simulate current and future wind power output[J]. Energy 2016;114:1224–39.
[32] Cole W, Karmakar A. Cost projections for utility-scale battery storage: 2023 update [R]. National Renewable Energy Lab (NREL), Golden, CO (United States), 2023.
[33] Chen X, Liu Y, Wang Q, et al. Pathway toward carbon-neutral electrical systems in China by mid-century with negative $CO_2$ abatement costs informed by high-resolution modeling[J]. Joule 2021;5(10):2715–41.
[34] CREEI (China Renewable Energy Engineering Institute). China renewable energy development report in 2022[R]. 2023. (in Chinese).
[35] Yi BW, Eichhammer W, Pfluger B, et al. The spatial deployment of renewable energy based on China's coal-heavy generation mix and inter-regional transmission grid[J]. Energy J 2019;40(4):45–74.
[36] Zhang Q, Chen W. Modeling China's interprovincial electricity transmission under low carbon transition[J]. Appl Energy 2020;279:115571.
[37] Zhuo Z, Du E, Zhang N, et al. Cost increase in the electricity supply to achieve carbon neutrality in China[J]. Nat Commun 2022;13(1):3172.